STUDY ON STRESS MANIFESTATION AND OVERLYING STRATA MOVEMENT LAWS UNDER DIFFERENT LITHOLOGICAL COMBINATIONS

by

Li LI *

China Energy Shendong Coal Group Co., Ltd,
Ecological Environment Management Center, Ordos, Inner Mongolia, China

Original scientific paper
https://doi.org/10.2298/TSCI2502107L

To gain insights into the impact of lithological and geometric configurations of Shendong strata on the propagation of damage within overlying rock layers, a model simulating overlying rock movement and damage propagation under varied lithological combinations was developed. The study involved four physical and seventeen numerical simulations to assess geological factors influencing strata behavior post-mining. Key findings include: Decreasing the thickness of the key stratum reduces the first weighting interval, accelerates fracture initiation, enlarges the subsidence area, and increases maximum subsidence; Raising the key stratum elevation diminishes both subsidence and its range, while delaying fracture initiation; Reducing mining thickness results in smaller pressure fluctuations, slightly extends the first weighting interval, and decreases both subsidence and its range; Enhancing key stratum hardness delays fracture occurrence, lowers the fracture zone height, and decreases the plastic zone volume.

Key words: *lithological combination, strata movement, key stratum modification, physical similarity experiment*

Introduction

Underground mines face significant challenges in maintaining safe operations and minimizing resource loss [1, 2]. Addressing these challenges requires a thorough understanding of roof movement, damage transmission in overlying strata, and damage propagation mechanisms. Lang *et al.* [3] simulated the height of the water-conducting fracture zone across different geological conditions at Xiaoji and Bulian Tower mines. Jin *et al.* [4] investigated the relationship between vertical stress and surrounding rock in reverse fault roofs under different lithology combinations in the context of working face thrust. Lin *et al.* [5] applied numerical simulations to create models under eight distinct lithological configurations, analyzing data on vertical stress and displacement in overlying strata. Zhu *et al.* [6] developed FLAC3-D models of floor responses under three lithological combinations, studying stress distribution, displacement, and damage depth. Teng *et al.* [7] observed the stress manifestation and overlying strata movement after water injection in Buertai coal mine. Miao *et al.* [8] applied rock mass fracture process analysis to explore fracture and collapse patterns of overlying strata with a thick key layer, while Zhu *et al.* [9] gathered extensive field data to understand differential deformation and failure in homogeneous *vs.* soft-hard rock floor combinations under mining pressure.

* Author's e-mail: 20029910@ceic.com

While these studies have advanced the theory of strata movement and damage control, research remains limited, highlighting the need for further exploration. This paper utilizes physical similarity and numerical simulation methods to examine overlying strata movement and damage propagation across various lithological combinations, offering insights into key stratum modification and strata control strategies for high intensity mining in western coalfields.

Overlying strata movement and stress manifestation laws

Initial weighting law

The critical span for the initial weighting of the main roof marks the point at which first weighting occurs as the working face advances after cutting initiation. This initial weighting causes either the collapse of the overlying strata or the subsidence of the roof. Figure 1 presents the mechanical model of a fixed-supported beam used to describe the mechanics of first weighting.

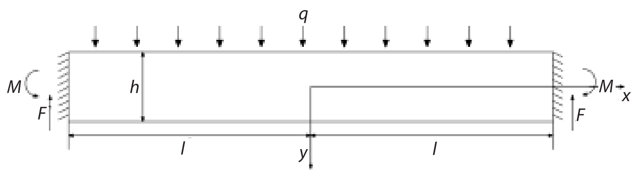

Figure 1. Mechanical analysis of fixed supported beams

Using the mechanical model depicted in fig. 1, the tensile stress and shear force expressions for the rock beam can be derived [4]:

$$\sigma_{al-2} = \frac{-6q}{h_3}x^2 y + \frac{4q}{h_3}y^3 + \left(\frac{2ql^2}{h_3} - \frac{3q}{5h}\right)y \tag{1}$$

$$\tau_{xy} = \frac{6q}{h_3}xy^2 - \frac{3q}{2h}x \tag{2}$$

where q is the load, h – the thickness of the fixed beam, and l – the fracture length of the beam.

A distribution cloud map of tensile and shear stresses inside the rock beam was generated using MATLAB, as shown in fig. 2.

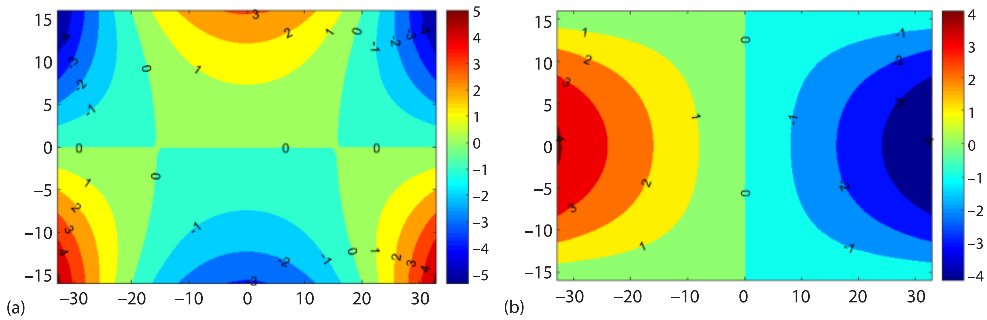

Figure 2. Distribution of tensile and shear stresses in fixed supported beams

The maximum tensile stress at the middle bottom position of the rock beam [6]:

$$\sigma_{\max} = \sigma_x \left| \left(0, h/2\right) \right. = \frac{q}{5} + \frac{ql^2}{h^2} \tag{3}$$

The ultimate span at which the rock beam fails [6]:

$$\sigma_{\max} = \sigma_x \left|\left(0, {}^{h}\!/\!_{2}\right) = \frac{q}{5} + \frac{ql^2}{h^2} \le \delta\left[\sigma_t\right] \right. \tag{4}$$

where σ_t is the ultimate tesile strength and δ – the softening index.

Periodic weighting law

Following the initial collapse of the overlying strata, continued advancement of the working face results in periodic collapses of the overlying strata, leading to intermittent weighting on the support structure. Figure 3 illustrates a cantilever beam mechanical model.

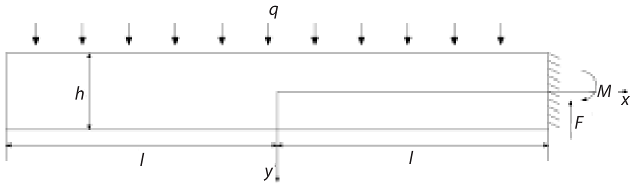

Figure 3. Mechanical analysis of cantilever beam

Tensile and shear stress expressions [8]:

$$\sigma_x = \frac{-6q}{h_3}(x+l)^2 y + \frac{4q}{h_3} y^3 - \frac{3q}{5h} y \tag{5}$$

$$\tau_{xy} = \frac{6q}{h_3}(x+l) y^2 - \frac{3q}{2h}(x+l) \tag{6}$$

Based on fig. 3, the maximum tensile stress at the co-ordinate (*l, –h/2*):

$$\sigma_{\max} = \sigma_x \left|\left(l, {}^{h}\!/\!_{2}\right) = \frac{3ql^2}{h^2} - \frac{q}{5} \right. \tag{7}$$

The ultimate span at which the cantilever beam remains free from tensile failure:

$$L_Z \le h\sqrt{\frac{\delta\left[\sigma_t\right]}{\eta q} + \frac{1}{15}} \tag{8}$$

The stress distribution in the cantilever beam was visualized as fig. 4.

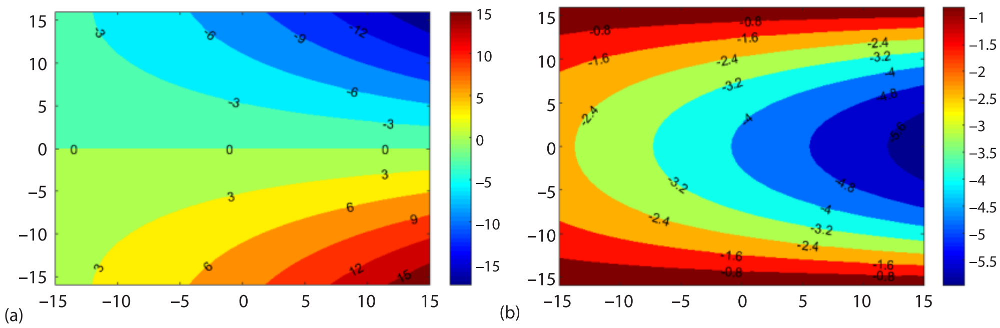

Figure 4. Distribution of tensile and shear stresses in cantilever beams; (a) tensile stress and (b) shear stress

Based on key stratum theory, a composite beam model is developed to evaluate the load exerted on the main roof [9]:

$$(q_n)_1 = \frac{E_1 h_1^3 \left(y_1 h_1 + y_2 h_2 + \cdots + y_n h_n \right)}{E_1 h_1^3 + E_2 h_2^3 + \cdots + E_n h_n^3} \tag{9}$$

where $(q_n)_1$ is the load of the nth strata on the first Stratum, h_i – the elastic modulus of the n^{th} Stratum, and γ_i – the volume force of the nth Stratum.

Geological conditions of the Shangwan coal mine in the Shendong mining area

Geological data from boreholes at the Shangwan coal mines were collected and summarized, including coal thickness, key stratum lithology, the distance between the key stratum and the coal seam, and the thickness of the key stratum, as illustrated in figs. 5(a)-5(c). The statistics reveal that coal seam thickness varies between 5 and 10 meters, with the majority of key strata composed of siltstone and a smaller proportion consisting of coarse sandstone. The distance from the key stratum to the coal seam predominantly ranges from 20-50 m, while the thickness of the key stratum spans from 20-55 m.

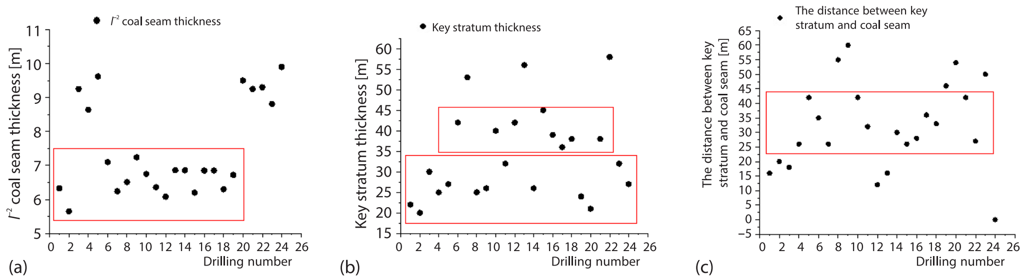

Figure 5. Geological data of Shangwan coal mines; (a) thickness data statistics, (b) key stratum thickness statistics, and (c) key stratum position statistics

Numerical simulation design and model parameters

Numerical simulations of overlying rock damage and stress field evolution were conducted using FLAC3D in fig. 6, reflecting the geological conditions and lithological combinations present at the Shangwan coal mine. The geometric model dimensions are set at 1000 m × 1000 m × 190 m. The working face measures 300 m in length in both the strike and dip directions. To mitigate boundary effects, 350 mwide boundary pillars were retained on both sides of the mining area. The failure of the overlying strata was simulated using the Mohr-Coulomb criterion, with displacement constraints applied to the front, back, and sides of the model.

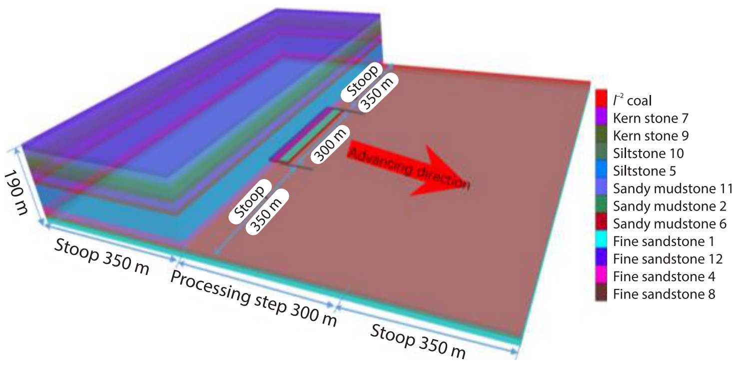

Figure 6. Numerical model diagram

Laws of structural failure of overlying strata under different lithological combinations

Influence of different key stratum thicknesses on the overlying strata stress field

As shown in fig. 7(a). As the working face advances to 50 m, the vertical stress measured 15 m ahead of the cutting eye initially decreases and then experiences a slight increase with rising key stratum thickness. This observation suggests that when the key stratum is thin, it fractures and collapses upon reaching the 50 m mark, resulting in stress concentration at the position 15 m ahead of the cutting eye. Conversely, as the key stratum thickness increases, the stratum does not fully fracture by the time the working face reaches 50 m, leading to an increase in vertical stress at that location. When the working face progresses to 200 m, the vertical stress at the same position shows an initial increase followed by a decrease as key stratum thickness increases.

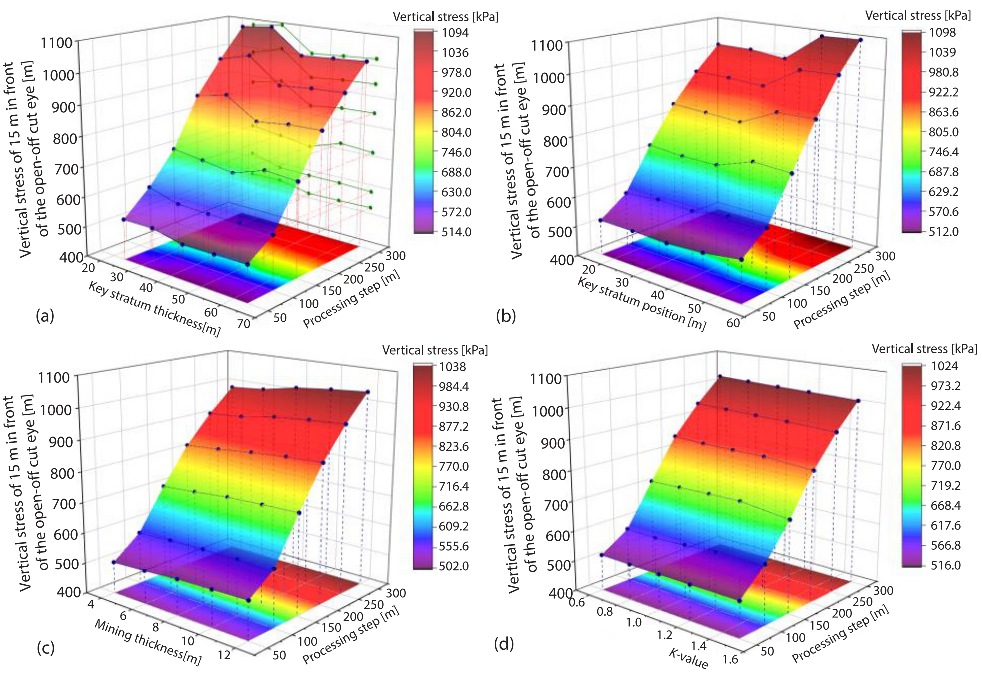

Figure 7. Comparative analysis of vertical stress at 15 m in front of open-off cut under different lithology combinations; (a) key stratum thickness, (b) key stratum position, (c) mining thickness, and (d) key stratum hardness

Influence of different key stratum positions on the overlying strata stress field

As the distance between the key stratum and the coal seam increases, the influence of mining on the key stratum diminishes, resulting in a delay in its fracture, which in turn leads to a decrease in vertical stress at that position, fig. 7(b). However, when this distance continues to expand, the disturbance to the key stratum from the working face becomes minimal upon reaching 100 m of advancement. The self-weight of the collapsed rock mass beneath the key stratum becomes more significant, causing an increase in vertical stress 15 m ahead of the cutting eye.

Consequently, the vertical stress at that position initially increases and then decreases as the distance between the key stratum and the coal seam increases.

Influence of different mining thicknesses on the overlying strata stress field

As illustrated in fig. 7(c), throughout the entire range of working face advancement from 50-300 m, the vertical stress measured 15 m ahead of the cutting eye exhibits an increase in response to the rising mining thickness. Furthermore, as the advancement distance increases, the vertical stress at that position also continues to rise. Notably, the vertical stress 15 m ahead of the cutting eye increases linearly with mining thickness.

Influence of different key stratum hardnesses on the overlying strata stress field

As presented in fig. 7(d), a larger K-value indicates a greater hardness of the key stratum. When the working face advances to 50 meters, the vertical stress measured 15 m ahead of the cutting eye initially decreases and subsequently stabilizes as K (key stratum hardness) increases. The increased hardness of the key stratum enhances its load-bearing capacity, resulting in a reduction of vertical stress at that location. As the working face advances to 200 m, the data depicted in fig. 7(d) show that the vertical stress at that position continues to decrease with increasing key stratum hardness. At this point, all key strata have fractured, and as the advancement distance increases, the vertical stress at that position first rises and then falls.

Conclusion

Decreasing the thickness of the key stratum results in a shorter first weighting step and intensifies the weighting effect. Elevating the position of the key stratum leads to a reduction in both subsidence. The vertical stress measured 15 m ahead of the cutting eye initially increases and then decreases as the distance of the key stratum from the coal seam increases, whereas the stress measured 45 m behind the cutting eye exhibits an opposite trend. Reduction of the mining thickness results in smaller fluctuations in pressure and a slight increase in the duration of the first weighting step. The vertical stress measured ahead of the cutting eye exhibits a linear increase with mining thickness, whereas the stress measured behind the cutting eye demonstrates a decreasing trend.

Nomenclature

E – Young's modulus of coal, [MPa]
h – thickness of the fixed beam, [m]
l – fracture length of the beam, [m]
q – load, [Pa]

Greek symbols

δ – softening index, [–]
σ_i – ultimate tesile strength, [Pa]

References

[1] Zhang, H., Exploring a New Path for the Development of the "Dual Carbon" Strategy in the Coal Industry (in Chinese), *Chinese Coal Industry Journal*, *2* (2022), pp. 32-35
[2] Teng, T., *et al*., Overburden Failure and Fracture Propagation Behavior under Repeated Mining, *Mining Metallurgy & Exploration*, *42* (2025), Jan., pp. 219-234
[3] Lang, Z. J., Feng, X., Research on the Influence of Lithological Combination Characteristics on the Height of Water Conducting Fracture Zones, *Journal of Energy Technology and Management*, *44* (2019), pp. 86-88
[4] Jin, B., *et al*., Study on the Activation Characteristics of Reverse Faults by the Combination Structure of Roof Lithology (in Chinese), *Chinese Journal of Mining and Technology*, *30* (2021), 3, pp. 172-180

[5] Lin, J. Y., *et al*., Research on Roof Mining Effect Under Different Lithological Combinations (in Chinese), *Journal of Guizhou University (Natural Science Edition)*, *36* (2019), 2, pp. 44-49
[6] Zhu, N. N., *et al*., Lithological Combination Effects Study of Mining Floor, Coal Technology, *36* (2019), 2, pp. 44-49
[7] Teng, T., *et al*., Water Injection Softening Modelling of Hard Roof and Application in Buertai Coal Mine, *Environmental Earth Sciences*, *84* (2025), 54
[8] Liao, X. X., *et al*., Analysis of Breakage and Collapse of Thick Key Strata Around Coal Face (in Chinese), *Chinese Journal of Rock Mechanics and Engineering*, *42* (2023), 5, pp. 1150-1161
[9] Zhu, S. Y., *et al.,* Restrictive Function of Lithology and Its Composite Structure on Deformation and Failure Depth of Mining Coal Seam Floor, *Journal of Mining & Safety Engineering*, *31* (2014), 1, pp. 90-96

Paper submitted: September 8, 2024
Paper revised: September 28, 2024
Paper accepted: October 12, 2024